Static and Dynamic Properties of Polymer Brushes at Moderate and High Grafting Densities: A Molecular Dynamics Study

Gui-Li He,† Holger Merlitz,*,† Jens-Uwe Sommer,‡ and Chen-Xu Wu†

Department of Physics and ITPA, Xiamen University, Xiamen 361005, P. R. China, and Leibniz Institut für Polymerforschung, D-01069 Dresden, Germany

Received April 29, 2007; Revised Manuscript Received June 24, 2007

ABSTRACT: We study static and dynamic properties of polymer brushes of moderate and high grafting densities using molecular dynamics simulations. The self-consistent-field theory is able to reproduce the observed density profiles once finite extensibility of the chains is included. A similar approach, using a Langevin-type model to account for a coupling between the vertical and lateral chain fluctuations, is successfully implemented to explain the lateral chain fluctuations at moderate-to-high grafting densities. The corresponding fluctuation dynamics in the direction lateral to the surface is well described by Rouse scaling. The dependence of the dynamics on grafting density (concentration) is very well described by the dynamic behavior of thermal blobs for the fluctuations in the direction both perpendicular and parallel to the surface. We find an anisotropic fluctuation dynamics related with two characteristic dynamic length scales in the both directions. We have further investigated the pulling forces acting on the polymer bonds. The force acting on the first bond directly connected to the surface is reduced at higher grafting densities, which is explained with an entropic contribution to the bond tension. A nonvanishing end-monomer tension is observed at high grafting densities. The integrated force (excess free energy) follows the prediction of the thermal blob model of the brush.

1. Introduction

Polymers grafted onto solid substrates have important applications in lubrication, adhesion, colloidal stability, and biotechnology. The special properties of such polymer brushes[1] are the result of the interplay of chain deformation (stretching), excluded volume effects (in particular solvent quality), and additional interactions such as polymer−substrate interactions (frequently of van der Waals type) and demixing effects in polymer brushes composed of different species (mixed brushes).[2] The complexity of such a many-body system limits its theoretical understanding to approaches such as mean-field solutions, ignoring fluctuation effects of real multichain systems.[3]

On the other hand, there is considerable interest in the dynamical behavior of polymer brushes to better understand the response to external fields and the nonequilibrium relaxation processes of brushes out of thermodynamic equilibrium. The knowledge of local forces acting on the polymer bonds is important for the control of brushes with high grafting densities. Moreover, information about the behavior of single grafted chains within the brush can be of interest for the development of composite systems, where functional groups or nanoparticles are attached to the free ends of the chains. Such questions are suitably addressed by computer simulations. In particular, molecular dynamics (MD) allows for the investigation of chain dynamics on realistic time scales. The neglect of hydrodynamic interactions is likely to deliver a reasonable approximation in the case of densely grafted polymers.

In the past, a number of computer simulations of grafted polymer systems have addressed various questions such as the scaling behavior of static quantities (brush height, density profiles, etc.).[4,5] For a recent overview, see ref 6. Extensive Monte Carlo simulations using the bond fluctuation model have been carried out by Lai, Wittmer, and Binder. Here, static and dynamic quantities such as the brush profile, last blob size, monomer fluctuations, and chain expulsion and exchange have been studied and compared to scaling and self-consistent-field (SCF) predictions.[7−9] Free energy profiles were simulated by Shaffer.[10] MD simulations of various static properties of brushes at low and moderate grafting densities were carried out by Murat and Grest.[11−13] Murat[14] and Bright[15] have carried out MD simulations of tethered chains under confinement. Brownian dynamics simulations have been applied by Neelov and Binder.[16]

In experiments, novel techniques like the living free radical polymerization have recently enabled researchers to construct brushes of very high grafting densities.[17−19] Since the majority of publications in the field of computational research had been focusing on brushes of low and moderate densities, there is an increasing demand for systematic simulations of high-density brushes as well. In order to investigate such systems, in this work we are using MD methods to study the behavior of grafted polymers up to very dense systems showing crystallization-like effects. In particular, we focus on quantities that have not been studied in more detail in previous work such as the lateral fluctuations of chains and the forces acting on the chain bonds. We test scaling predictions using, among other approaches, the semidilute solution model for the polymer brush. We find that at higher grafting densities monomer fluctuations are laterally much more confined as compared to the scaling model, a phenomenon which can be explained by a coupling effect between the lateral fluctuations and the stretching of the chains in the direction perpendicular to the surface. A nonvanishing end-monomer tension, observed at high grafting densities, is further reducing the lateral mobility of the chain ends. Their dynamics in the brush state is controlled by "diving" events on a long time scale. This is of particular importance for novel experiments and applications, where functional groups or nanoparticles are

* Corresponding author. E-mail: merlitz@gmx.de.
† Xiamen University.
‡ Leibniz Institut für Polymerforschung.

10.1021/ma070983l CCC: $37.00
Published on Web 08/14/2007

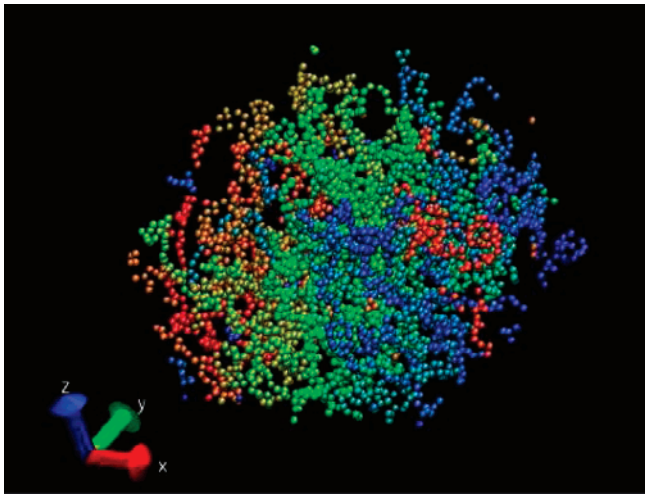

Figure 1. Typical brush conformation with $N = 64$ monomers and grafting density $\sigma = 0.059$. Different colors are used for graphical reasons and do not have any physical relevance.

attached to the chain ends. On intermediate time scales, dynamic scaling is well obeyed without corrections of the monomer friction constant except for very high grafting densities.

The rest of the work is structured as follows: in section 2, we briefly describe the simulation method. In section 3.1, a summary of several static properties of the brushes, including a comparison with mean-field (SCF) predictions, is presented. Significant deviations are observed in the case of the vertical distributions of the end monomers, which are then linked to the lateral fluctuation behavior of these monomers in section 3.2. In section 3.3, we investigate the diffusion dynamics of chain ends. In section 3.4, the bond stretching forces and potentials are analyzed, and our conclusions are given in section 4.

2. Methods

As a tool to study polymer brushes, the LAMMPS molecular dynamics package[20] was employed. The polymer chains were made of coarse-grained bead−spring monomers and end-grafted to form a 8×8 grid on a flat surface which defined the $x-y$ plane of the system. Periodic boundary conditions were applied in $x-y$ direction, whereas the grafting surface was featuring a short-range repulsive potential. Throughout the paper, Lennard-Jones (LJ) units are used, based on the monomer diameter $\sigma = 1$, the binding energy $\epsilon = 1$, and the mass $m = 1$ (compare with eq 2). This model is very similar to systems used in earlier MD studies, e.g., by Grest,[13] but the particular set of simulation parameters was taken from Bright et al.,[15] who have also used LAMMPS as their simulation platform.

The total potential acting on a monomer can be described as the sum

$$U_{\mathrm{TOT}} = U_{\mathrm{LJ}} + U_{\mathrm{FENE}} + U_{\mathrm{WALL}} \tag{1}$$

Here, the first term stands for the pair interaction, a LJ potential with cutoff at its minimum and a shift such that only repulsive contributions remained:

$$U_{\mathrm{LJ}} = 4\epsilon\left(\left(\frac{\sigma}{r}\right)^{12} - \left(\frac{\sigma}{r}\right)^{6} - \left(\frac{\sigma}{r_c}\right)^{12} + \left(\frac{\sigma}{r_c}\right)^{6}\right) \tag{2}$$

where $r_c = 2^{1/6}\sigma$ is the cutoff distance. The second term in eq 1 is a finite extensible nonlinear elastic (FENE) spring potential, which is creating the connectivity between the monomers. The FENE potential used in this work is defined as follows:

$$U_{\mathrm{FENE}} = -0.5KR_0^{\,2}\ln\left[1 - \left(\frac{r}{R_0}\right)^2\right] + 4\epsilon\left[\left(\frac{\sigma}{r}\right)^{12} - \left(\frac{\sigma}{r}\right)^{6}\right] + \epsilon \tag{3}$$

where the first term is attractive and allows for a maximum bond length of $R_0 = 1.5\sigma$, whereas the second term, a LJ potential, contributes a short-range repulsion, which is cut off at $2^{1/6}\sigma$, the minimum of the LJ potential. The spring constant was chosen to be $K = 30\epsilon/\sigma^2$. For uncharged chains, this parameter set leads to an average bond length of $l_{\mathrm{av}} = 0.97\sigma$.[14] The last term in eq 1 is the repulsive wall potential

$$U_{\mathrm{WALL}}(z) = \epsilon\left[\frac{2}{15}\left(\frac{\sigma}{z}\right)^9 - \left(\frac{\sigma}{z}\right)^3\right] \tag{4}$$

This wall is located at $z = 0$, the same height as the grafted monomers, and the potential was cut off at a $z_c = \sigma$, with exception of section 3.4, where we investigate the bond forces near the wall. Here, the potential was cut at its minimum to avoid any singularity of the force.

The equation of motion of each nongrafted monomer is given by the Langevin equation:

$$m\frac{\mathrm{d}^2\mathbf{r}_i}{\mathrm{d}t^2} + \varsigma\frac{\mathrm{d}\mathbf{r}_i}{\mathrm{d}t} = -\frac{\partial U_{\mathrm{TOT}}}{\partial \mathbf{r}_i} + \mathbf{F}_i \tag{5}$$

where $m = 1$ is the monomer mass, $\mathbf{r}_i$ is the position of the ith monomer, ζ is the friction coefficient, and $\mathbf{F}_i$ is a random Gaussian force with the correlation function $\langle F_i^{\alpha} F_j^{\beta}\rangle = 2k_{\mathrm{B}}T\zeta\delta^{\alpha\beta}\delta_{ij}$. Here, the Greek indices denote the spatial components of the force, k_{B} is Boltzmann's constant, and T is the absolute temperature. For our simulations, $T = 1.2\epsilon$ was chosen, a time step of $\Delta t = 0.0015\tau$, where $\tau = \sigma(m/\epsilon)^{1/2} = 1$ is the LJ time, and a friction constant of $\zeta = \tau^{-1}$, the same set of simulation parameters as used in earlier MD studies.[15]

3. Results

The initial brush conformation was set up as an array of stretched chains. Then, 10^7 simulation steps were carried out for relaxation, followed by several 10^7 simulation steps for data production. Figure 1 displays a typical brush conformation after relaxation. It was noticed that the relaxation into static structural properties, as discussed in section 3.1, took place quite rapidly within a few million simulation steps. Certain dynamical properties of the system, like the relaxation of the vertical (z) component of the radius of gyration, however, as discussed in section 3.3, displayed rather long autocorrelation times of the order of 10^6-10^7 time steps for the $N = 64$ brushes, depending on grafting density. In the case of $N = 128$, the decay of the corresponding autocorrelation function took even longer and required almost 1 order of magnitude more simulation steps. Consequently, brushes of length $N = 128$ with very high grafting densities remained excluded from investigations of sections 3.2 and 3.3, where long relaxation times could otherwise deliver inaccurate results within feasible simulation times.

3.1. Density Profiles. A simplified model of polymer brushes was presented by Alexander and de Gennes,[21,22] where the brush was regarded as a stretched array of correlation (thermal) blobs, whose size is given by

$$\xi \sim \sigma^{-1/2} \tag{6}$$

the average distance between neighbored monomers grafted at density σ. Within the blobs, (nearly) unperturbed excluded volume conformations are assumed:

$$\xi \sim g^{\nu} \tag{7}$$

where g denotes the number of monomers contained in a blob and ν is the Flory exponent in 3D. The height of the brush then equals the number of blobs times their size, and the density profile is a step function which drops sharply at the surface of the brush. Later, a more accurate model was developed by Semenov[23] and Milner et al.[24] using self-consistent-field (SCF) arguments. The SCF theory was subsequently extended to cover high brush densities by Shim et al.[25] and Lai et al.[26] The "classical" theory of polymer brushes has been further addressed by Netz and Schick.[27] In this section, some of the structural properties of the simulated brushes are compared with predictions of the corresponding SCF approximations.

Figure 2 displays the rescaled monomer densities of several brushes over the rescaled z-coordinate. The plots roughly fall onto a master curve, which deviates from the simplified step function of the Alexander model (AM). The standard (Gaussian) SCF theory by Milner et al., henceforth denoted as SCF (MWC), predicts a parabolic shape:

$$\frac{\phi(z)}{\sigma^{(3-1/\nu)/2}} = \frac{\pi^2}{8w}(H^2 - Z^2)\,\Theta(H - Z) \tag{8}$$

where $H = h/(N\sigma^{(1-\nu)/(2\nu)})$ is the rescaled height h of the brush, $Z = z/(N\sigma^{(1-\nu)/(2\nu)})$ the rescaled vertical coordinate, and w the third virial coefficient under athermal solvent conditions; this parameter as well as the rescaled height H were left as free parameters when fitting eq 8 to the data (dotted curve). Here and in the following we use Flory's value $\nu = 3/5$ for simplicity instead of the more exact value ($\nu = 0.588$), which results in $1/2(3 - 1/\nu) \simeq 2/3$ (0.65) and $(1 - \nu)/2\nu \simeq 1/3$ (0.35). The difference is not essential for the scaling results of those properties discussed in this paper.

The SCF (MWC) model describes the density distribution qualitatively, although not perfectly well. In fact, the drop of monomer density at the surface of the brush is sharper than predicted by SCF theory but softer than predicted by the AM. The results are very similar to earlier Monte Carlo studies at high grafting densities,[4] indicating that both simulation techniques (MC and MD) are delivering consistent structural predictions for these systems.

In previous work it has been argued that deviations from the SCF profile could be caused by a substantial contribution of the last blob.[6,8,9] It should be noted that in the present simulations we use chains which are, at $N = 128$, comparably long. Grest[13] has used chains as long as $N = 200$ (although at low grafting densities), but nevertheless deviations from the SCF profile were considerable and the scaling of the profile displayed systematic deviations. However, the SCF theory was modified by Shim and Cates[25] to account for the finite extensibility of the chain. These non-Gaussian corrections to the SCF (MWC) equations become increasingly important at high grafting densities, where the chains are overstretched. The resulting equations, which are henceforth denoted as SCF (SC) equations, have to be evaluated numerically and contain a parameter γ which we have used as a free variable to fit the simulation data. The best coincidence was found with the choice $\gamma \approx 7$ (Figure 2, solid curve for $\sigma = 0.31$). Actually, the value of γ should be near the topological dimension of space, i.e., $\gamma = 3$, but the corresponding curve did not represent the data very well. Shim et al. have found similar deviations while making comparisons with lattice calculations, though toward the other direction. (They found $\gamma \approx 1$ to fit the data more accurately at high grafting densities.) In fact, their best value for γ turned out to be a function of the grafting density, a phenomenon we have observed as well during the analysis of our simulations. As Shim et al. pointed out, these shifts are a consequence of the nonuniversality of their strong-stretching corrections to the Gaussian elastic limit. It therefore appears adequate to use γ as a free parameter to fit simulation results.

Figure 3 displays the density profile of the end monomers. In this case, a rescaling did not create any master curve, a result also observed in previous Monte Carlo simulations[4] at high grafting densities. The SCF (MWC) theory would predict

$$\frac{\psi(z)N}{\sigma^{2/3}} = \frac{\pi^2}{2w} Z(H^2 - Z^2)^{1/2}\Theta(H - Z) \tag{9}$$

which is plotted as a dotted curve and which is qualitatively different from the observed behavior. During the simulations, the vertical coordinates of the monomers appear to be more rigid and are peaking sharply around their average positions. The inclusion of finite extensibility with the SCF (SC) model (the same $\gamma = 7$ parameter was used as was in Figure 2) delivers a result that comes qualitatively close to the simulations (solid curve, for $\sigma = 0.31$) but does not describe the data in a fully quantitative manner. As will be discussed later in this paper, the chains at high densities experience an additional end-monomer tension which is further reducing the end-point fluctuations of the chain.

Figure 4 displays the average vertical coordinate $\langle z_k \rangle$ of the kth monomer along the chain, rescaled with the corresponding value of the end monomer. Here, Gaussian SCF (MWC) theory predicts

$$\frac{\langle z_k \rangle}{\langle z_N \rangle} = \sin\left(\frac{k\pi}{2N}\right) \tag{10}$$

For different brush densities, the results do not fall nicely onto a master curve. As could be expected, lower brush densities were closer to the SCF prediction, but the high densities displayed an increasing deviation from Gaussian mean-field theory.

3.2. Lateral Fluctuations. The litmus test for scaling models of polymer brushes is the fluctuation behavior of the chains in the direction parallel to the surface. Here, two competing models have been suggested: the Alexander model (AM)[21] and the semidilute solution model (SDM).[28] Both of them regard the chain as a string of correlation blobs.[29] But the AM assumes these blobs to be uniformly stretched perpendicular to the grafting surface, whereas the SDM allows for a free diffusion of the blobs in lateral direction which is considered to be decoupled from the extension of the chains in the directed perpendicular to the surface. This has consequences to the lateral (horizontal) distributions of monomers with respect to their grafting points: Be $\rho^2 = \langle (x - x_g)^2 + (y - y_g)^2 \rangle$ the average mean-squared lateral fluctuation of the monomer with respect to the grafting point of the chain (x_g, y_g). Following the AM, each monomer is allowed to move freely only inside the tube formed of the array of correlation blobs, whose size is scaling as $\xi \sim \sigma^{-1/2}$, which implies $\rho^2 \sim \sigma^{-1}$, with no dependence on the number of monomers N. According to the SDM, the blobs

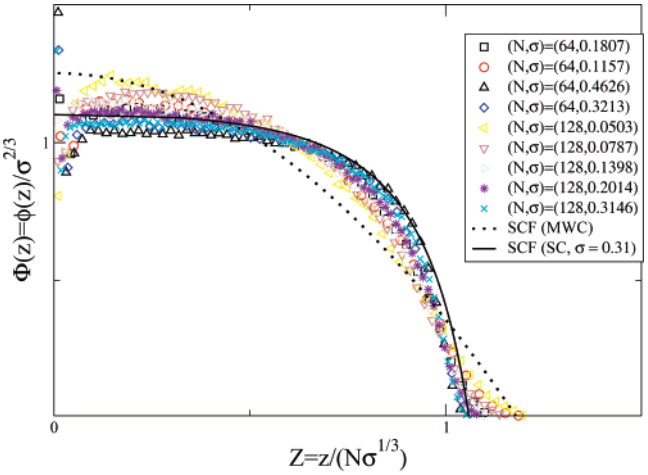

Figure 2. Rescaled density distribution plotted vs rescaled distance from the substrate. N is the number of monomers per chain, and σ is grafting density. The profiles roughly fall onto the same master curve, indicating that the corresponding systems were located inside the brush regime. The dotted curve is the Gaussian SCF prediction (eq 8); the solid curve includes finite extensibility corrections for $\sigma = 0.31$.

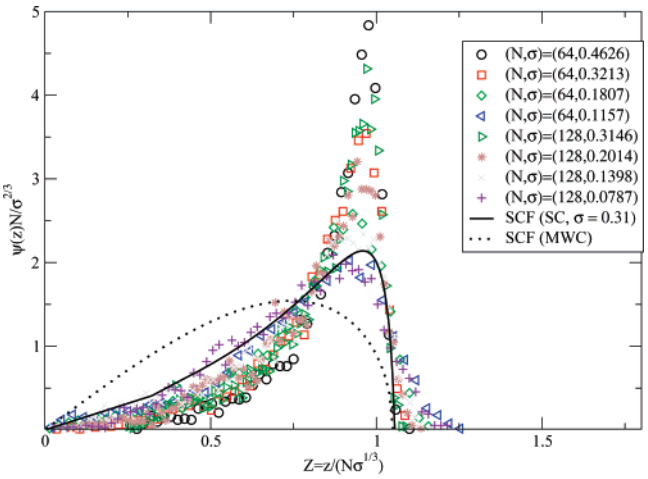

Figure 3. Rescaled end-monomer density distribution plotted vs rescaled z-coordinate. Brushes of different grafting densities do not fall onto a master curve, and the Gaussian SCF prediction of eq 9 (dotted line) is unable to match the data. Finite extensibility corrections deliver more realistic, although not fully quantitative, predictions (solid curve, $\sigma = 0.31$).

are allowed to carry out a random walk inside the brush. Using eqs 6 and 7, we obtain

$$\rho^2 \sim \frac{N}{g}\xi^2 \sim N\xi^{2-1/\nu} \sim N\sigma^{(1/2\nu)-1} \sim N\sigma^{-1/6} \qquad (11)$$

Thus, according to the SDM, the lateral fluctuations are proportional to N and depend weakly on σ.

As long as only the excluded volume interactions are relevant and ξ is much larger than the monomer size, a general scaling behavior can be expected as follows:

$$\frac{\rho^2}{\rho_0^2} = f_\rho(\sigma/\sigma^*) \qquad (12)$$

where ρ_0^2 denotes the value of ρ^2 for a single chain (mushroom), i.e., $\rho^2(\sigma = 0)$. The result of eq 11 follows from eq 12 if we require $\rho^2 \sim N$ in the limit $\sigma/\sigma^* \gg 1$. In Figure 5, we display our results for both brushes ($N = 64$ and $N = 128$) and several grafting densities in the scaling as suggested by eq 12. For the

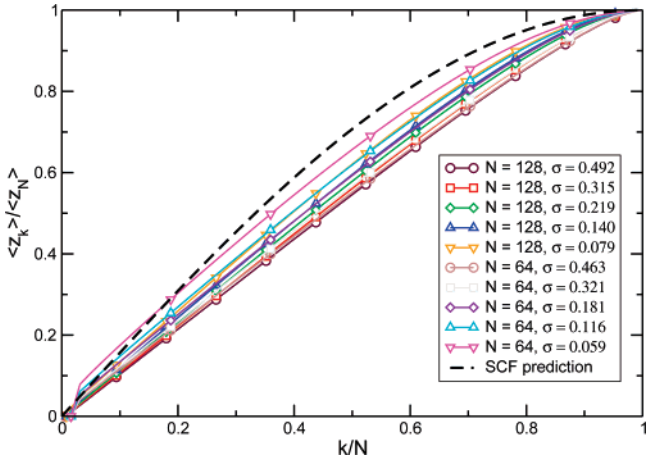

Figure 4. Average vertical coordinate $\langle z_k \rangle$ of the kth monomer along the chain, rescaled with the corresponding value of the end monomer. The dashed curve is the SCF prediction (eq 10).

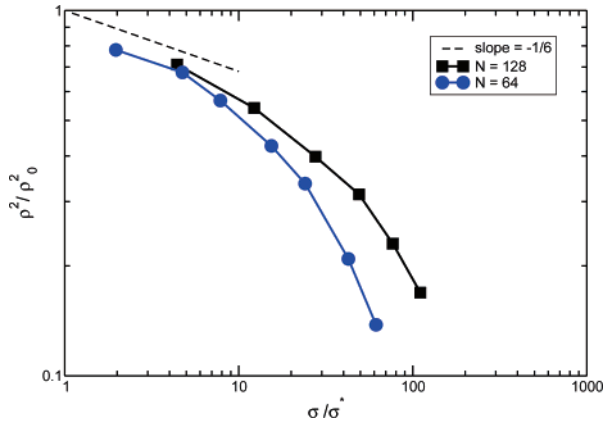

Figure 5. Mean-squared lateral fluctuations of the end monomers, scaled according to eq 12.

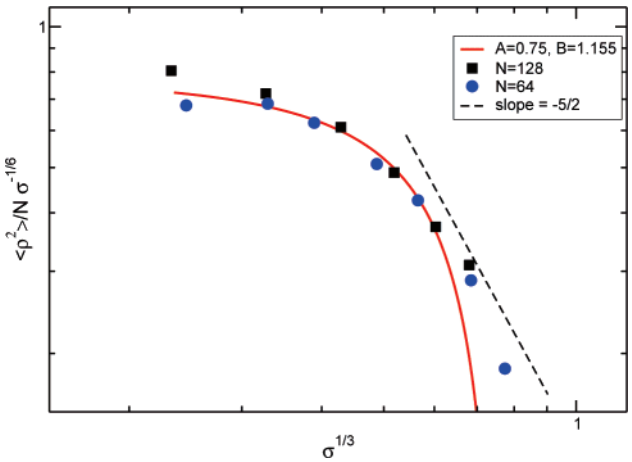

Figure 6. Mean-squared (lateral) fluctuations of the end monomers reduced by the scaling prediction and plotted against $\sigma^{(1-\nu)/(2\nu)}$. The result of the freely jointed chain model (Langevin model) is indicated by the solid curve together with the fit parameter used. The Alexander model is indicated by the slope of $-5/2$ in this representation.

overlap concentration we used $\sigma^* = 1/\rho_0^2$. Full scaling is approached only within the low-density regime rather close to the overlap threshold. For higher brush densities we observe a splitting of the curves which is related to a downturn of both curves from the slope predicted in eq 11 by the SDM.

In Figure 6, we compare our results with the prediction of eq 11. Here, the lateral mean-squared fluctuations are rescaled by $N\sigma^{-1/6}$ and plotted against $\sigma^{1/3}$. If the SDM were valid for

all grafting densities, a straight horizontal line was expected. Again, this can only be observed for low grafting densities. At higher grafting densities, the curves bend down following a behavior which is apparently independent of the overlap density and depends only on the actual grafting density. Beyond that, the slope is gradually decreasing to approach the slope predicted by the AM (dashed line).

These results suggest the SDM to be asymptotically correct only within a limited regime of moderate brush densities, near the crossover to the mushroom state. A possible explanation for the observed drop-down of lateral fluctuations as compared to the prediction of the SDM could be the finite extensibility of real chains or more generally a coupling between the lateral fluctuations and the stretching of the chains in the direction perpendicular to the surface. For the ideal Gaussian chain, fluctuations into different spatial directions are decoupled. In the SDM, such a decoupling of chain statistics according to the Gaussian model of the coarse-grained (blob chain) is tacitly assumed. For real chains, however, an extension of the chain in one direction (*z*-direction perpendicular to the surface) should reduce the fluctuations in other directions ($x-y$ plane parallel to the surface).

In order to investigate this effect in detail, let us assume that the chain is composed of $n = N/g$ segments of length ξ. Considering this effective chain as a freely jointed chain, we obtain for the lateral fluctuations

$$\rho^2 = n\xi^2\{1 - L_2[L_1^{-1}((H/\xi)/n)]\} \tag{13}$$

where $L_1(x) = \coth(x) - 1/x$ and $L_2(x) = 1 - \coth(x)/x + 2/x^2$ denote Langevin functions (L_1^{-1} being the inverse of L_1). Using the scaling relations between g, ξ and σ, as given in eqs 6 and 7, we obtain

$$\frac{\rho^2}{N\sigma^{1/(2\nu)-1}} = B\{1 - L_2[L_1^{-1}(A\sigma^{(1-\nu)/(2\nu)})]\} \tag{14}$$

where A and B are constants which cannot be obtained from scaling.

The predicted behavior according to eq 14 is plotted as a solid curve in Figure 6. Here, we used a best fit of the two parameters A and B to the observed data. Apparently, the finite extensibility of the chain could in principle explain the deviations of the lateral fluctuation behavior for higher grafting densities. If the grafting density becomes very high (last two data for $N = 64$ and last data point for $N = 128$), the curves deviate, which can be explained by the failure of the semidilute blob scaling as assumed in the derivation of eq 14. Here the blobs become very small, and the bare chain should be considered rather than the coarse-gained blob chain. These data for high grafting densities approach the behavior of the AM which, on the other hand, corresponds to the fully stretched chain of blobs.

Finally, we note that these results are not changed when considering a center monomer instead of the end monomer. This is not surprising since the size of the last blob ξ_l is much smaller (and independent of chain length) compared with the total lateral fluctuations as predicted by the SDM.

3.3. Dynamics of Individual Chains. A more detailed view on the behavior of polymer brushed can be obtained when investigating the dynamics of individual chains. Again, the SDM can be applied to obtain a model for the dynamics of the segmental fluctuations. Our simulations can reveal the true polymer dynamics on time scales larger than the characteristic fluctuation time of a coarse-grained segment (which can be considered to be of the order of the size of a Kuhn segment here) and without hydrodynamic interactions.

We start with the lateral fluctuation dynamics. Again, when considering the chain as an ideal chain of blobs, the characteristic time of the chain's fluctuations will be the Rouse time, which is given by

$$t_R = \tau_\xi (N/g)^2 \tag{15}$$

where τ_ξ denotes the characteristic relaxation (or diffusion) time of the blob of size ξ comprising g monomers. On the other hand, without hydrodynamic interaction we have

$$\tau_\xi \sim g^{2\nu+1} \sim \sigma^{-1-1/2\nu} \sim \sigma^{-11/6} \tag{16}$$

where we have used the dynamical exponent $2\nu + 1$ for a Brownian chain without hydrodynamic interactions and eqs 6 and 7. This leads to $t_R \sim N^2\sigma^{-1/6}$.

In order to test dynamical scaling, we need the characteristic length scale which is related to the Rouse relaxation time. Let us call it the *characteristic dynamic length scale* (DLS). For the lateral fluctuation the DLS should be given by the mean-squared fluctuations. Therefore, we assume for the dynamic scaling relation

$$\frac{\rho^2(t)}{\rho_0^2} = f_\rho(t/t_R) \tag{17}$$

with $\rho^2(t) = \langle (x(t)) - x(0))^2 + (y(t) - y(0))^2\rangle$. Here, $x(t)$ and $y(t)$ denote the actual positions of monomers at time t. In Figure 7, our simulation data are displayed using the dynamic scaling prediction for the end monomers of the chains. The curves follow dynamic scaling in a good approximation. However, for the highest grafting densities, deviations are observed. Here, also the lateral fluctuations are strongly constrained beyond the scaling predictions as has been discussed in the previous section. For high grafting densities, the fluctuations of the monomers hardly exceed the blob diameter and the dynamic scaling assumption made above must fail.

Next, we consider the mean-squared displacement of the end monomers in the direction perpendicular to the surface. In this case the average extension (brush height) is not the DLS: The external field (and thus any stretching) is neglected when estimating the Rouse time in the ideal chain model (and thus in the coarse-grained blob chain). The Rouse equation in the effective field approximation has been discussed by Johner and Joanny.[30]

The existence of a characteristic length scale larger than the DLS, namely the brush height, gives rise to a second characteristic time scale longer than t_R. Lai et al.[5] have suggested a time scale t_H defined as the time required for the autocorrelation function to drop to a fraction of $1/e \approx 0.37$ of its initial value. Their Monte Carlo study at the Θ-point suggested a N^3 dependence of $\tau(R_{gz})$ on chain length and approximately $\sigma^{1.6}$ dependence on grafting density. A simple argument for this relation is based of the center-of-mass diffusion constant of the chain. Assuming this to follow the Rouse behavior $D \sim 1/N$ delivers a characteristic time t_H for exploring the full brush height which is proportional to N in a diffusive process. This immediately yields $t_H \sim N^3$, a relation which has been approved analytically in ref 30.

Table 1 contains our results t_H (column 3), which should be regarded as being only approximative, since the data generally displayed a more complex decay rather than just a single

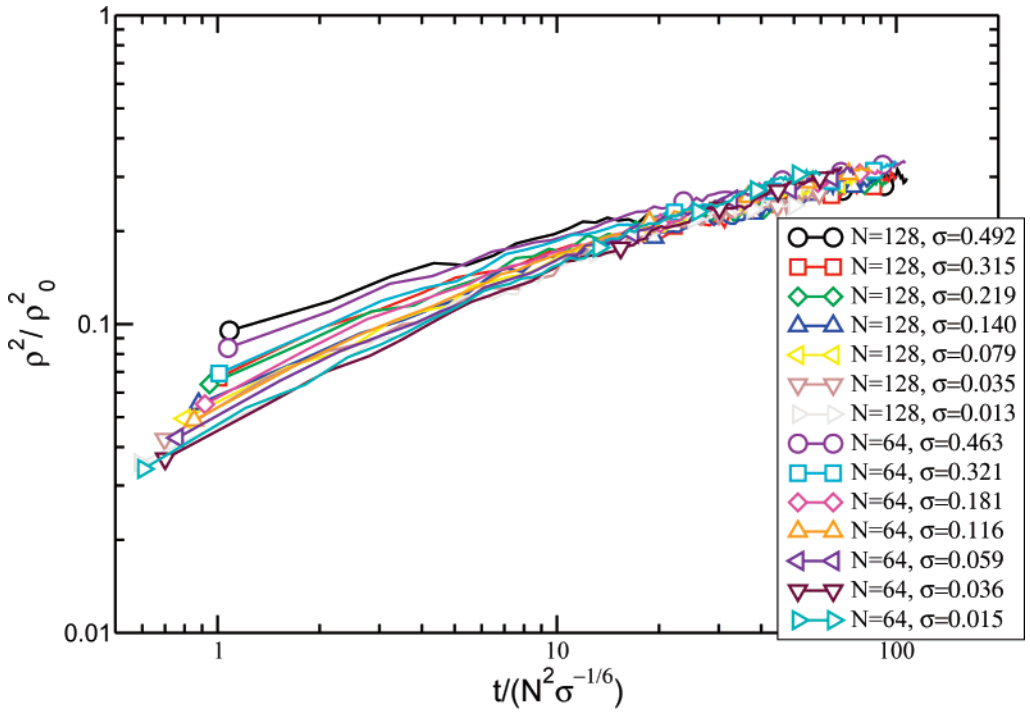

Figure 7. Squared displacements of the end monomers in lateral direction. Time scales are given in units of MD time steps, and length scales are given in LJ units.

Table 1. Dynamics of Vertical Brush Fluctuations[a]

N	σ	t_H	τ(cycle)	N(cycle)
64	0.0590	1.1	0.32	10
	0.116	1.3	0.61	4.6
	0.181	1.8	0.95	2.5
	0.321	3.7	2.0	0.85
	0.463	10	3.5	0.36
128	0.0787	10	2.4	0.86
	0.140	12	4.5	0.35
	0.219	16	6.7	0.15
	0.315	≈25	>8	≈0.06

[a] σ is the grafting density, t_H the relaxation time of the z-component of the radius of gyration (in 10^6 time steps), τ(cycle) the average diving cycle time of the end monomers (in 10^6 time steps), and N(cycle) the average number of diving cycles (per chain and 10^7 time steps).

negative exponential. They show that t_H of the longer brushes are in fact roughly a factor of 8 larger compared to the shorter brushes, supporting the claimed N^3 dependence. The data also show that t_H initially increases slowly with σ, but very rapidly at high grafting densities, which indicates a qualitative change of the system's relaxation dynamics when crossing over from semidilute concentrations to the high grafting density regime.

Since the DLS for this process is unknown, we apply dynamic scaling only on the scale of the correlation blobs. Since the Rouse time is rather large (and the time scale t_H even larger) there is a broad region for $t \ll t_R$ where no chain length dependence is expected. Rescaling our data according to $\langle(z(t) - z(0))^2\rangle/\xi^2$ and t/τ_ξ results in the plot obtained in Figure 8. This gives a very good mastering of data except for the highest grafting densities. Since no other assumption than dynamic scaling of the correlation blobs has been made, our data support the SDM. Furthermore, the data show that the effective monomer friction coefficient is not changing for moderate grafting densities in the absence of hydrodynamic interactions. Here, MC simulations may display a different behavior.[5]

The long time dynamics in a brush requires the end of the chain to "dive" into the brush domain, a process which becomes increasingly inhibited at high brush densities. For a quantitative analysis of this process, we define a diving cycle as follows: Be $\langle z\rangle$ the average vertical coordinate of the end monomer. Then, τ(cycle) is defined as the recurrence time of the end monomer at $\langle z\rangle$ under the condition that the threshold $0.7\langle z\rangle$ has been passed. In other words, the end monomer of the chain has to dive into the brush and reach a depth of $0.7\langle z\rangle$ at least. Upon its return back to the surface, the cycle time is the time that has passed since the end monomer had last touched $\langle z\rangle$ prior to its dive. The threshold of $0.7\langle z\rangle$ is arbitrary, of course, and chosen in order to collect a sufficient number of diving events at high grafting densities within feasible simulation times.

Table 1 contains the cycle time τ(cycle) and the average number of cycles N(cycle) per chain and 10^7 time steps. The cycle times are increasing roughly linear with the grafting density. The frequencies of these cycles, however, are dropping very rapidly, so that the average time for a chain spending in such a diving cycle is going down. As will be demonstrated in section 3.4, there exists a nonvanishing end-monomer tension at high grafting densities. This tension might be imposing an energy barrier which prevents the chain ends from diving easily into the brush domain.

The analysis of these diving processes delivers an alternative point of view to describe the increasing rigidity of the brush at high grafting densities. It delivers time scales about how long the end monomer is in contact with either the free solvent or the concentrated polymer solution of the brush. These times are of relevance for a novel class of experiments, in which functional groups or nanoparticles are attached to the chain ends.

3.4. Chain Energy and Bond Force. Polymer brushes are usually obtained by forming chemical bonds between an end group of the chain and (possibly functionalized) surface sites. Knowing the dependence of the bond forces on the grafting density is important to develop strategies for creating brushes with high grafting densities. The method of MD allows to calculate the average vertical forces pulling on the chains and the corresponding grafting energies.

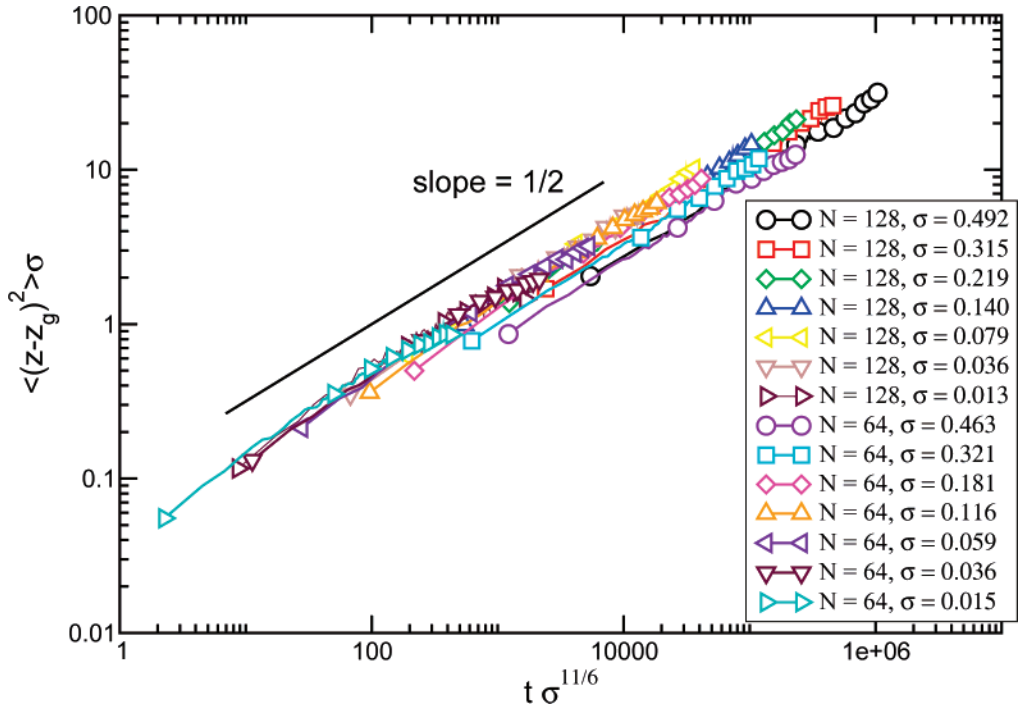

Figure 8. Squared displacements of the end monomers in vertical direction. Time scales are given in units of MD time steps, and length scales are given in LJ units.

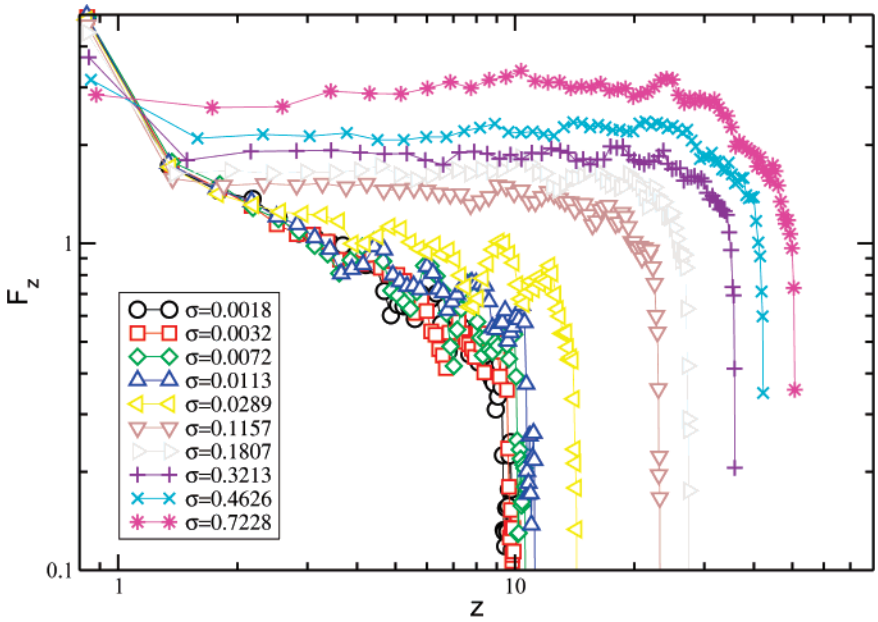

Figure 9. Averaged bond forces along the *z*-direction for $N = 64$ as a function of the distance from the surface.

Here, the length r of each bond was analyzed and the FENE potential eq 3 used to compute the spring force, yielding

$$\mathbf{F} = \langle \nabla U_{\mathrm{FENE}}(\mathbf{r}) \rangle$$

$$= \left\langle -\mathbf{r}\left(\frac{KR_0^2}{r^2 - R_0^2} + \frac{4\epsilon}{r^2}\left[12\left(\frac{\sigma}{r}\right)^{12} - 6\left(\frac{\sigma}{r}\right)^{6} \right] \right) \right\rangle \qquad (18)$$

In Figure 9, the vertical (z) component of this force is plotted for $N = 64$ chains as a function of the average z-coordinates of the involved monomers. At the top of the brush, the stretching forces vanish, as long as the grafting density remains moderate. At high grafting densities, even the end bond displays some residual stretching as a result of strong pair interactions with neighbored chains, an observation also reported in refs 27 and 30.

The first bond, connecting the grafted monomer with the first movable monomer, exhibits particularly high stretching forces. Interestingly, these were found to be decreasing at higher grafting densities. In order to investigate this phenomenon in more detail, different wall potentials were implemented and simulations at various grafting densities were carried out. Figure 10 shows the resulting averaged stretching forces $\langle F_z(\sigma) \rangle$. When

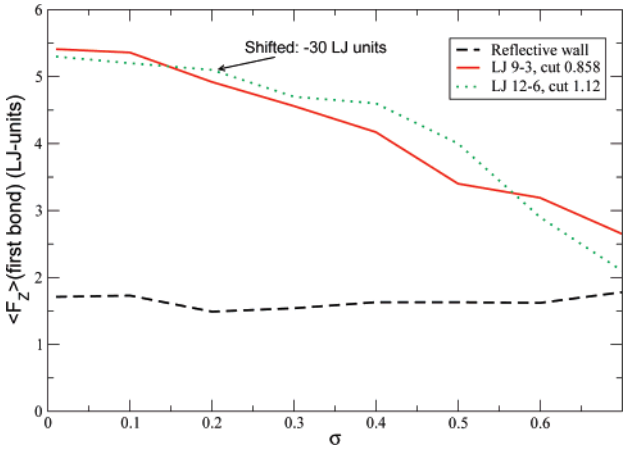

Figure 10. Forces acting on the bond between the grafted monomer and the first mobile monomer along the *z*-direction, using different models for the wall potential. After removal of a 30 (LJ units) offset from the LJ 12−6 curve, it falls roughly onto the LJ 9−3 curve.

using a reflective wall, no systematic variations of $\langle F_z(\sigma)\rangle$ were visible. Once LJ wall potentials were employed, which were cut off at their minimum and shifted, such that only a repulsive contribution remained, the stretching forces displayed a drop off toward higher densities. The total force was much higher in the case of the LJ 12−6 potential, which is both harder and of longer range than the 9−3 potential, but after shifting it by −30 LJ units both curves were on top of each other. It was further noted that the values became invariant on the chain length once chains of $N > 8$ segments were used, which indicates local fluctuations to be responsible for this phenomenon.

In fact, the reduction of the first bond length with increasing density can be explained as an entropic effect: The LJ potentials of the wall extend into the positive *z*-direction, and their repulsive forces impose geometric constraints to the motion of the second monomer. If we assume that, at a given bond length, the first bond is restricted to rotate within a cone with a half angle θ_0 above the surface ($\theta_0 = 0$, indicating free rotation within a half-sphere), then this angle would decrease (i.e., the entropy would increase) with increasing bond length. This entropic effect hence leads to an additional contribution to the first bond force. With increasing grafting density, however, the mobility gained by entropic overstretching is lost as a result of steric restrictions imposed by neighbored monomers. This can be verified using the second moment of the orientation fluctuations:

$$P_2(z) = \frac{3}{2}\left(\langle \cos^2\theta\rangle - \frac{1}{3}\right) \tag{19}$$

Here, the angle θ denotes the angle between the bond and the vertical (*z*) direction. For an ensemble of free Gaussian chains, this quantity would be zero, and finite values are indicating a reduced amount of fluctuations of the bond orientation. In Figure 11, it is plotted for the first bond, using the LJ 9−6 wall potential. First, one may notice the high value of the second moment even at low σ—the restrictions imposed by the repulsive wall potential. We may estimate this restriction in terms of the half angle θ_0 as

$$P_2 = \frac{1}{2}\frac{\sin^3(\theta_0)}{1-\sin(\theta_0)} \tag{20}$$

In order to reach the value of $P_2 \simeq 0.6$, we obtain $\theta_0 \simeq 45°$. With increasing grafting density, the monomer's mobility

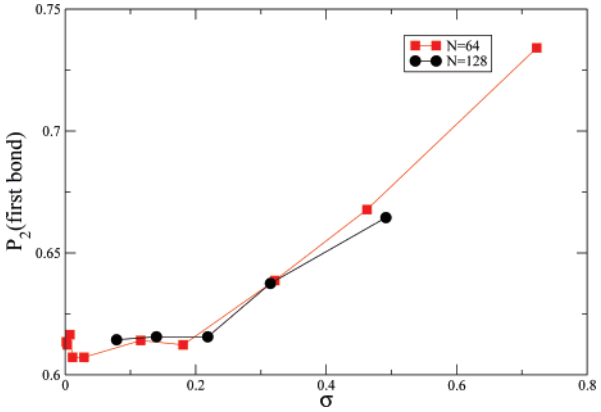

Figure 11. Fluctuations of the orientation of the bond between the grafted monomer and the first mobile monomer for the LJ 9−3 potential (compare with eq 19).

becomes even further restricted due to pair interactions with neighbored chains, creating the observed increase of P_2. In this situation, the entropic overstretching of the first bond begins to diminish, since it would not lead to any increase of the angular space which is accessible to the second monomer. As a result, the entropic contribution to the bond force, which, according to Figure 10, amounts to roughly 3 LJ units, disappears at high grafting densities, and the bond force is dropping. In the case of the reflective wall, however, there is no repulsive potential which would extend into the positive half-sphere, and hence it does hardly affect the second monomer's mobility. The above-discussed entropic contribution to the stretching is therefore absent, and no dependence of the force on grafting density is visible.

Although the observed effect is related to the coarse-grained model (beads and springs), an analogous steric effect may as well be present in the case of real chains grafted onto a molecular surface.

The total stretching energy of each chain is obtained by integrating the force curve in Figure 9. First, we note that the force calculated is a thermodynamic force including all entropic (fluctuation) effects. This is obvious when recalling the singular behavior of the geometrically most constrained first bond. Thus, the integrated force corresponds to the excess free energy F_{exe} of the chain compared to the (isotropic) state of the free chain in the bulk. Since each blob corresponds to a thermal energy of the order of k_BT, we obtain

$$F_{\text{exe}} \sim \frac{N}{g} \sim N\sigma^{1/2\nu} \sim N\sigma^{5/6} \tag{21}$$

In Figure 12, we plot the excess free energy for both chain lengths (scaled with *N*) as a function of σ. The curves fall onto a master curve and display a sublinear behavior in agreement with eq 21.

Our observations may point toward an unexpected implication: It is generally believed that brushes, if grafted to high densities, become thermodynamically less stable because of the increased stretch of the chains and, consequently, a high value of their excess energy. A desorption of the grafted monomer from its substrate would, however, rather be caused by the peak value of the force pulling on its bond than the free energy difference of the entire chain. This may imply that, at high grafting densities, where the entropic contribution to the bond force is absent, the brush would become rather stabilized regardless of the amount of free energy stored in the system.

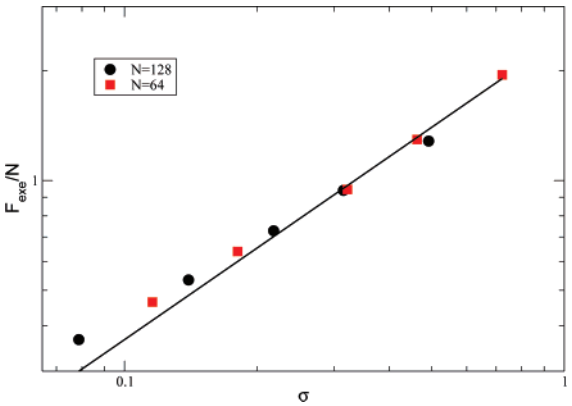

Figure 12. Excess free energy, scaled with N, for different grafting densities. The line corresponds to a slope of 5/6 (eq 21).

In this context it may be interesting to note that experimental approaches which allow to create covalently attached polymers at high grafting densities are of the so-called "grafted from" type, as opposed to the "grafted to" approach.[17,18] Starting from an initiator monolayer, the brush is grown layer by layer, and the grafting density is high at any stage of the process. To create the dense initiator layer, the Langmuir−Blodgett deposition technique is used. Here, the monolayer is initially floating in the solvent and subsequently deposited while passing the substrate through the film. The first polymer layer is then grown simultaneously onto the dense initiator layer, and if the grafting density is high enough to suppress lateral fluctuations of these monomers, the entropic forces, as discussed in this paragraph, cannot contribute to the stretching forces pulling at the anchor point. Using this approach, Devaux et al.[17] have achieved a stretch of 0.7−0.9 (fraction of contour length), which corresponds to the highest brush densities simulated in the present work.

4. Conclusions

In this work, polymer brushes up to high grafting densities and of chain lengths ($N = 64$ and $N = 128$) were investigated using molecular dynamics simulations. In agreement with previous simulation studies, the static properties of brushes deviate from the Gaussian SCF (MWC) model, in particular with respect to the end-point distribution of chains. The inclusion of finite extensibility of the chains with the SCF (SC) model delivers a much better coincidence with the data, but this model is not fully universal and requires the optimization of a system-dependent parameter.

On the other hand, using the thermal blob size $\xi \sim 1/\sigma^{1/2}$ as a basis for a scaling description yields a good agreement with the simulation results. Here, the fluctuation behavior of the chains in the direction parallel to the surface is significant for the model of the brush. We found that at low grafting densities the random walk scaling and thus decoupling between the degrees of freedom of the chains in the different spatial directions remain valid. For higher grafting densities, however, the lateral fluctuations become increasingly confined. This observation can, again, be explained by the finite extensibility of the chains and thus a coupling between the chain statistics in the different spatial directions. A Langevin model fits the behavior of the lateral fluctuations fairly well.

The model of correlation blobs can be extended to dynamical quantities such as the diffusion properties of the monomers in the brush. We have found a very good agreement of our data for the mean-square displacement of the end monomers with the dynamic scaling assumption. Here, the diffusion dynamics within a correlation blob is assumed to follow the behavior of excluded volume chains without hydrodynamic interactions. Appropriate rescaling of time and length scales leads to mastering of the dynamical data for times shorter than the Rouse time of the chain. Only for high grafting densities, deviations from this scaling behavior are found, which could be related to an increasing monomer friction coefficient as a result of increasing pair interactions. To obtain the dynamical crossover scaling for times longer than the Rouse time, a knowledge of the characteristic dynamic length scale is necessary. In particular, for the dynamics in the direction perpendicular to the surface, this length scale does not correspond the chain extension but is much smaller. Stretching of chains in this direction creates a second characteristic time scale which scales like the third power of the chain length as already proposed by several authors. We find our data for the autocorrelation function of the vertical component of the radius of gyration to be in agreement with this prediction.

The stretching of chains inside the brush regime can be monitored using the forces acting on the bonds in z-direction (Figure 9) and the corresponding total bond energies (Figure 12). The latter are scaling with the chain length N and sublinearly with the grafting density. For high grafting densities, a nonvanishing end-chain tension is observed. The forces pulling on the first bonds are particularly strong, but dropping with increasing grafting density as a result of a reduced entropic contribution to the chain energy. The reason for this result can be related to the specific geometric constraints which are experienced by the first bead near the surface. Stretching the bond creates a larger available solid angle for bond fluctuations. On the other hand, at higher concentrations, the pressure exerted by the other monomers reduces the available bond angle and also the stretching of the first bond. Although this effect is related to the coarse-grained model (beads and springs), an analogous steric effect should be expected for real chains as well. This suggests that, in contrast to common believe, brushes may become increasingly stable at high grafting densities. Moreover, the force distribution shows a plateau-like behavior for higher grafting densities.

Acknowledgment. This work was partly supported by the National Science Foundation of China under Grant 10225420. G.-L. He and H. Merlitz thank J.-U. Sommer for the hospitality during a research stay at the IPF Dresden.

References and Notes

(1) One should call grafted polymers a brush if the grafting density is high enough to force the chains to elongate and orient considerably in the direction perpendicular to the surface.
(2) Sidorenko, A.; Minko, S.; Schenk-Meuser, K.; Duschner, H.; Stamm, M. Switching of polymer brushes. *Langmuir* **1999**, *15*, 8349.
(3) Marko, J. F.; Witten, T. A. Phase separation in a grafted polymer layer. *Phys. Rev. Lett.* **1991**, *66*, 1541.
(4) Chen, C.-M.; Fwu, Y.-A. Monte Carlo studies of polymer brushes. *Phys. Rev. E* **2000**, *63*, 011506.
(5) Lai, P.-Y.; Binder, K. Structure and dynamics of polymer brushes near the θ point: A Monte Carlo simulation. *J. Chem. Phys.* **1992**, *97*, 586.
(6) Binder, K. Scaling concepts for polymer brushes and their test with computer simulations. *Eur. Phys. J. E* **2002**, *9*, 293.
(7) Lai, P.-Y. Grafted polymer layers with chain exchange: A Monte Carlo simulation. *J. Chem. Phys.* **1993**, *98*, 669.
(8) Wittmer, J.; Johner, A.; Joanny, J. F.; Binder, K. Chain desorption from a semidilute polymer brush: A Monte Carlo simulation. *J. Chem. Phys.* **1994**, *101*, 4379.
(9) Binder, K.; Lai, P.-Y.; Wittmer, J. Monte Carlo simulations of chain dynamics in polymer brushes. *Faraday Discuss.* **1994**, *98*, 97.
(10) Shaffer, J. S. Free-energy profiles ans scaling in polymer brushes. *Phys. Rev. E* **1994**, *50*, R683.

(11) Murat, M.; Grest, G. S. Structure of a grafted polymer brush: A molecular dynamics simulation. *Macromolecules* **1989**, *22*, 4054.
(12) Grest, G. S.; Murat, M. Structure of grafted polymeric brushes in solvents of varying quality: A molecular dynamics study. *Macromolecules* **1993**, *26*, 3108.
(13) Grest, G. S. Grafted polymer brushes: A constant surface pressure molecular dynamics simulation. *Macromolecules* **1994**, *27*, 418.
(14) Murat, M.; Grest, G. S. *Phys. Rev. Lett.* **1989**, *63*, 1074.
(15) Bright, J. N.; Stevens, M. J.; Hoh, J.; Woolf, T. B. Characterizing the function of unstructured proteins: Simulations of charged polymers under confinement. *J. Chem. Phys.* **2001**, *115*, 4909.
(16) Neelov, I. M.; Binder, K. Brownian dynamics simulation of grafted polymer brushes. *Macromol. Theory Simul.* **1995**, *4*, 119.
(17) Devaux, C.; Cousin, F.; Beyou, E.; Chapel, J.-P. Low swelling capacity of highly stretched polysterene brushes. *Macromolecules* **2005**, *38*, 4296.
(18) Tsujii, Y.; Ohno, K.; Yamamoto, S.; Goto, A.; Fukuda, T. Structure and properties of high-density polymer brushes prepared by surface-initiated living radical polymerization. *Adv. Polym. Sci.* **2006**, *197*, 1.
(19) Advincula, R. C., Brittain, W. J., Caster, K. C., Rühe, J., Eds.; *Polymer Brushes;* Wiley-VCH: Weinheim, 2004.
(20) Plimpton, S. J. Fast parallel algorithms for short-range molecular dynamics. *J. Comput. Phys.* **1995**, *117*, 1.
(21) Alexander, S. *J. Phys. (Paris*) **1977**, *38*, 977.
(22) deGennes, P. G. *Macromolecules* **1980**, *13*, 1069.
(23) Semenov, A. N. *JETP Lett.* **1985**, *85*, 733.
(24) Milner, S. T.; Witten, T. A.; Cates, M. E. *Macromolecules* **1988**, *21*, 1610.
(25) Shim, D. F. K.; Cates, M. E. Finite extensibility and density saturation effects in the polymer brush. *J. Phys. (Paris)* **1989**, *50*, 3535.
(26) Lai, P.-Y.; Halperin, A. Polymer brush at high coverage. *Macromolecules* **1991**, *24*, 4981.
(27) Netz, R. R.; Schick, M. Classical theory of polymer brushes. *Europhys. Lett.* **1997**, *38*, 37.
(28) Halperin, A. On polymer brushes and blobology: An introduction. In Briuinsma, R., Rubin, Y., Eds.; *Soft Order in Physical Systems;* Plenum Press: New York, 1993.
(29) deGennes, P. G. *Scaling Concepts in Polymer Physics;* Cornell University Press: Ithaca, NY, 1979.
(30) Johner, A.; Joanny, J. F. Dynamics of polymeric brushes: End exchange and bridging kinetics. *J. Chem. Phys.* **1993**, *98*, 1647.

MA070983L